Journal of Computational Physics **173,** 527–548 (2001)
doi:10.1006/jcph.2001.6891, available online at http://www.idealibrary.com on IDEAL®

Particle Simulation of the Neoclassical Plasmas

J. A. Heikkinen,* T. P. Kiviniemi,† T. Kurki-Suonio,† A. G. Peeters,‡ and S. K. Sipilä†

*VTT Chemical Technology, Euratom-TEKES Association, P.O. Box 1404, FIN-02044 VTT, Finland; †Helsinki University of Technology, Euratom-TEKES Association, FIN-02015 HUT, Finland; and ‡Max-Planck-Institut für Plasmaphysik—EURATOM Association, D-85748 Garching, Germany
E-mail: Jukka.Heikkinen@vtt.fi

Received September 25, 2000; revised May 2, 2001

A 5D Monte Carlo particle simulation method for advancing rotating plasmas in tori is presented. The method exploits the neoclassical radial current balance (quasineutrality condition). Including the ion polarization current gives the time rate of change of the radial electric field and related evolution of the rotation velocity components. A special orbit initialization for a quiescent start and an efficient radial flux solving algorithm with reduced numerical noise are developed. Numerical stability of the method with respect to the strength of the perpendicular viscosity and Mach number of the poloidal rotation is investigated. This new approach enables one to separate the nonambipolar transport characteristics from the ambipolar ones. Because nonambipolar transport can support sheared flows, this model can provide a very efficient tool for studying transport barriers and related neoclassical mechanisms in toroidal plasmas.

Key Words: Monte Carlo simulation; plasma; transport.

I. INTRODUCTION

While neoclassical toroidal plasmas have been extensively studied theoretically, only a few global numerical simulations of such plasmas exist. However, in high-performance tokamak discharges the plasma conditions can seriously challenge the analytical expressions for the neoclassical transport. Various effects including toroidicity, details of the collision operator, convection and inertia, rotation, finite ion orbits, steep plasma gradients, and boundary conditions push neoclassical theory to its limits. On the other hand, simulations in which transport is assumed highly anomalous and is modeled by transport coefficients calculated from various turbulence models are becoming inadequate now that the transport in various improved confinement regimes can approach the neoclassical level. Therefore, there is a growing need for a reliable numerical simulation of neoclassical plasmas.

0021-9991/01 $35.00

Local test particle simulations with Monte Carlo collision operators have been applied to evaluate the transport coefficients [1] in both tokamaks and helical devices. Here, some main elements of the neoclassical transport, such as particle or heat diffusion either by toroidal ripple or by collisions between unlike particles (including alpha particle, impurity, and other minority ion transport), have been identified to be generally in good agreement with the neoclassical theory in appropriate limits. However, neither the neoclassical ambipolar electric field nor the momentum or energy conserving collisions fundamental for a proper evolution of the neoclassical plasma has been simulated in any of these works. The latter collisions require parallel processing of a large amount of particles, which has become practical only very recently. Recent advances in computer efficiency have made global particle simulations feasible in small- and medium-size toroidal plasma configurations [2].

The development of gyrokinetic particle models [3], based on drift orbits of electrons and ions in tokamak geometry and including finite Larmor radius effects and magnetic mirroring forces, has allowed the investigation of self-consistent particle orbits and electrostatic potential fluctuations, together with basic neoclassical properties [4] of such plasmas. However, because of the dominance of turbulence in determining plasma transport characteristics, many of the neoclassical mechanisms either cannot be discriminated or are sacrificed by various assumptions for greater computing speed.

Lin *et al.* [8] carried out steady-state, multispecies simulation of neoclassical transport using a linearized, time-varying weighting δf-scheme [5] with Monte Carlo collision operators corrected for conservation of momentum and energy. However, as the total distribution f was not resolved, the ambipolar radial electric field and rotation dynamics were not found. Methods that use the total f-technique [6–8] can, in principle, model the true charge separation of ions and electrons and solve the ambipolar electric field. However, these conventional gyrokinetic algorithms have so far been applied only to studies of low-frequency microinstabilities and related turbulent transport in tori. This has been accomplished by using (to improve the computing speed) the assumption of adiabatic electron distribution or by neglecting collisions, thus eliminating the neoclassical ambipolar field and rotation. Whenever the electron distribution has been assumed fixed or electrons have been followed according to drift-kinetic approximation, ambipolar modes have been found from the solutions of the gyrokinetic Poisson relation [9]. However, no results for the global neoclassical plasma dynamics and equilibrium have been presented. Three-dimensional gyrokinetic simulations clarifying the interaction of the neoclassical ambipolar field and turbulence-generated field are in preparation [10] and should illustrate the time evolution of the field.

In the present work, an alternative approach to a consistent simulation of neoclassical plasmas is presented. In this approach the radial electric field is solved from the radial current balance (quasineutrality condition). This corresponds to resolving the gyrokinetic Poisson relation essentially in the limit of $\mathbf{k} = 0$; i.e., all electrostatic modes with finite wave vector $\mathbf{k}$ are neglected. This enables us to obtain the true neoclassical balance, because the ambipolar microinstability generated diffusion not affecting the radial current balance is filtered out. The dynamics of the radial electric field E_r can be obtained directly from the ion polarization drift, which is proportional to $\partial E_r/\partial t$. Recently, this technique was successfully applied when the relaxation of E_r to equilibrium with an appearence of geodesic acoustic modes was investigated [11].

A global analysis that includes finite gradients in the background parameters is not possible by analytical means but requires particle simulation. The present scheme for solving

E_r provides a general way of finding the neoclassical equilibrium for arbitrary plasma cross section, tokamak aspect ratio, and background gradients, and it avoids all the numerical complications (by sacrificing the turbulence physics) arising from solving the Poisson relation correct to all **k**. It is shown that such important problems as orbit loss (and biased probe) or poloidal rotation generated by background gradients at an L–H transition [12] together with the related radial electric field dynamics can be self-consistently and directly solved with the present numerical method. The scheme is essentially a total f-method, and it is implemented with an option for a binary collision operator [13] that conserves momentum and energy pairwise in collisions suitable for total f-methods only. These conservation properties are fundamental in proper treatment of the rotation dynamics and neoclassical transport in general. The δf-method provides low noise only for problems in which deviations from Maxwellian distribution are small. However, in the present problem, the deviations can be large as a result of steep gradients and the presence of an ion orbit loss mechanism. Thus, the low noise δf-technique is not suitable for this problem since disturbances from Maxwellian are most probably large.

The paper is organized as follows: The neoclassical radial current balance and the method for solving the radial electric field are introduced in Section II. This is followed by a description of the numerical implementation of the method in Section III. The initialization schemes and the algorithms for resolving the fluxes and advancing the electric field, as well as the stability issues of the method, are discussed. Section IV presents both global and annular simulation results for Physical Tokamak-2 FT-2 [14] and Axially Symmetric Divertor Experiment ASDEX Upgrade [15] tokamaks showing both spatial and temporal numerical convergence for the calculated radial electric field at transport barrier transition conditions. The conclusions are given in Section V.

II. RADIAL CURRENT BALANCE

In neoclassical plasmas, a radial electric field arises because of different diffusion rates of ions and electrons. This electric field ensures quasineutrality and makes the radial fluxes of electrons and ions equal [16] (also a consequence of automatic ambipolarity in the case of axisymmetry and momentum conservation in collisions). This flux corresponds to the flux arising from ion–electron collisions. In the present particle simulation method, the radial electric field $E_r = \langle E_r(\rho,\theta)\rangle = -(d\Phi(\rho)/d\rho)\langle|\nabla\rho|\rangle$ on a magnetic surface with the coordinate ρ is evaluated from the condition $\langle j_r\rangle = 0$ for the radial current density j_r. A general geometry of the simulations is depicted in Fig. 1. The condition $\langle j_r\rangle = 0$ has to hold for all values of ρ and time t. Here, $\langle\cdots\rangle$ denotes the flux surface average, and θ is the poloidal angle.

In the following, radial flux arising from ion–electron collisions is not considered because it causes only ambipolar diffusion, which does not affect the radial current balance. As helical systems are not considered, the electron current remains small and is neglected. The radial current density is therefore

$$j_r(\rho,\theta) = j_{NC} + j_{\text{visc}} + j_{\text{pol}}, \tag{1}$$

where the terms on the right-hand side correspond, respectively, to neoclassical radial ion current (arising from standard guiding-center drifts, excluding the polarization drift), gyroviscosity current, and polarization current. The polarization drift is a real guiding-center drift. Here, j_{pol} is written separately from j_{NC} because it depends on $\partial E_r/\partial t$, which is to be solved. In the simulation, the current j_{visc}, which is not a genuine guiding-center drift,

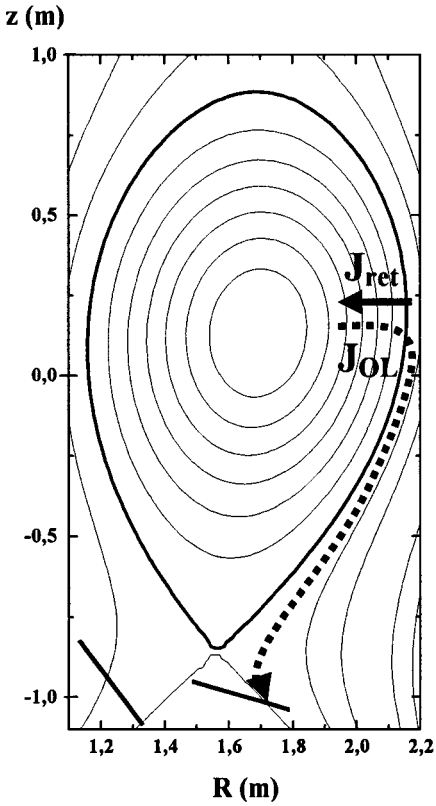

FIG. 1. Poloidal cross section of the (axisymmetric) toroidal simulation geometry. Contributions from orbit loss and return current for the radial current balance are shown.

and $j_{\rm pol}$ can be generated by assigning, locally, each ion the following radial drift velocities (keeping θ and toroidal angle intact during the corresponding drift step) [17]:

$$v_{\rm visc} = -(\eta/\Omega B)[\partial^2 E_r(\rho,\theta)/\partial\rho^2]|\nabla\rho|^2, \tag{2}$$

$$v_{\rm pol} = (1/\Omega B)\partial E_r(\rho,\theta)/\partial t. \tag{3}$$

Here, $\Omega = eB/m$ is the cyclotron frequency of an ion with charge e and mass m, and B is the magnetic field calculated locally at (ρ,θ). The perpendicular (gyro)viscosity coefficient is given by [18] $\eta = \eta_{Br} \equiv (3/10)k_B T \nu_{ii}/m\Omega^2$, and the ion–ion collision frequency is $\nu_{ii} = e^4 \ln\Lambda n/(4\pi\epsilon_0^2 m^2 v_T^3)$, where $\ln\Lambda$ is the Coulomb logarithm, ϵ_0 is the vacuum permittivity, and n and T are the density and the temperature of the ions, respectively.

It should be noted that $v_{\rm visc}$, unlike the other drifts considered, does not arise from the drift of individual ions, but is estimated as averages of the bulk plasma behavior. Its true form would require resolving the gyromotion (and possibly turbulence), which would make the simulation too CPU-expensive. Thus, we rather treat it in an order-of-magnitude sense using Eq. (2). The bulk ion rotation speed $v_\perp$ binormal to the magnetic field (perpendicular to the magnetic field and tangential to the magnetic surface) is approximated by the $\mathbf{E}\times\mathbf{B}$ flow velocity in this direction. This is well justified because the viscosity drift becomes important only for binormal rotation speeds much larger than the diamagnetic flow speed. This should capture the first-order effects of the gyroviscosity.

For an ion ensemble, the polarization current can be written as $\langle j_{\rm pol}\rangle = \alpha(\rho)\partial\langle E_r(\rho, \theta)\rangle/\partial t$, where

$$\alpha(\rho) = e\sum_i \frac{|\nabla\rho|(\rho_i, \theta_i)}{\Omega(\rho_i, \theta_i)B(\rho_i, \theta_i)} \frac{p_i}{\langle|\nabla\rho|\rangle} \frac{1}{dV(\rho)}, \tag{4}$$

and $\sum_i$ denotes the sum over all ions in the ensemble with positions ρ_i, θ_i within the flux surface volume element dV at ρ. p_i is the weight factor equal to the total number of ions in a real configuration represented by the ith test particle. Thus, E_r can be solved from the equation

$$\partial E_r/\partial t = -(1/\alpha)\langle j_{NC} + j_{\rm visc}\rangle \tag{5}$$

on flux surface ρ at time t. This equation is valid for all collisionality regimes. Adding the viscous drift velocity to the guiding-center motion is not essential for deriving Eq. (5). It is rather a small correction which may have some effect in regions where the electric field changes extremely rapidly, e.g., as a result of the applied boundary condition. This perpendicular Braginskii viscosity [18] is not present in the gyro-center equations since it is not a real guiding-center drift, but is a fluid term related to the gyration of an ensemble of particles. Since it affects the current, it is included in the motion of particles. It should be noted that the neoclassical enhancements, related to the inertia in poloidal rotation [19], are hidden in their complete form in j_{NC}, and do not appear explicitly in the currents $\langle j_{\rm visc}\rangle$ and $\langle j_{\rm pol}\rangle$.

The total current j, in steady-state ($j_{\rm pol} = 0$), consists of j_{NC} and $j_{\rm visc}$. j_{NC} itself consists of many different components; two of them are shown in Fig. 1 for an interesting case of radial current balance near a separatrix of a tokamak. Since $j_{\rm visc}$ is small in general, a so-called return current $j_{\rm ret}$ driven by an inward radial electric field and the orbit loss current $j_{\rm OL}$ are the main components of current balance at the edge. These current components, however, are carried out by the same test particles and cannot be separated in the code. In the simulation, the particle guiding-centers in an ensemble are followed in a drift-kinetic formalism in the presence of a full collision model operator. Some of the particles hit the divertor or material wall and, thus, phenomenologically, it is possible to talk about loss current. This current component is balanced by the return current to which these loss particles may have earlier contributed or may contribute again after their reinitialization. The power of the present simulation method is that there is no need to make any separation between the return and torque driving currents.

The present method is incomplete in the sense that the poloidal electric field cannot be solved simultaneously in a consistent way. Although the latter can in many cases be neglected to a good accuracy, and it seldom plays a dominant role in neoclassical physics, if so desired, the poloidal variation of the electrostatic potential $\Phi(\theta)$ on a magnetic surface may be included to a satisfactory accuracy by taking adiabatic perturbation of distribution of electrons $\delta n_e = (n_0 e/k_B T_e)(\Phi - \langle\Phi\rangle)$ and using quasineutrality condition on the surface. In the following, the inclusion of the poloidal electric field is not investigated. There are no problems in extending the present method to helical systems where electrons in addition to ions may play an important role in the current balance.

III. PARTICLE SIMULATION MODEL

The core of the present method for solving E_r is the evaluation of the ion radial current, i.e., the right-hand side of Eq. (5). This can be accomplished by accumulating the net radial ion motion in test particle simulations. We have implemented our method into the Monte Carlo particle-following code ASCOT [20]. In ASCOT, each particle is followed along its guiding-center orbit determined by the $\mathbf{E} \times \mathbf{B}$, gradient and curvature drifts, collisions, polarization, and gyroviscosity drifts. The particle following takes place in a realistic geometry, e.g., in the one shown in Fig. 1, including the region outside the separatrix. Magnetic background data are imported in the code only in two dimensions (neglecting toroidal dependence), but the toroidal ripple can be included in the analysis by assuming a sinusoidal perturbation $\delta B = B\delta \sin(N\phi)$ to the magnitude of the magnetic field (see, e.g., Ref. [23]). Thus, calculations are not necessarily based on an axisymmetric tokamak model. In the ASCOT code, the guiding-center equations are written in straight magnetic field line coordinates [23] using canonical Hamiltonian variables to avoid numerical drifts. The magnetic background is assumed stationary. In simulations of evolution of E_r on a time scale that is fast compared to the evolution of the background by particle transport, electrons can be assumed to provide a stationary neutralizing background and are not simulated. Because the calculation of E_r is based on the balance of radial currents, no ambipolar processes are included. Therefore, as already mentioned in Section II, also the ion–electron collisions are neglected. Figure 2 shows the flow chart of the ASCOT code.

For fixed E_r, the adopted numerical model has been recently tested in Refs. [21, 22] by calculating poloidal rotation relaxation rates for a homogeneous plasma and by comparing the perpendicular conductivity and parallel viscosity evaluated by ASCOT with the analytical expressions in Refs. [25, 28]. The simulations were carried out for a wide range of collisionalities and rotation velocities. Qualitative and, also, rough quantitative agreement was found, but some differences were identified to arise from simplifications made in the analytical theory.

In solving the radial electric fields from neoclassical current balance, three essential parts of the code are (a) orbit integration, (b) collision model, and (c) subroutine which solves E_r from the flux of particles (evaluated from guiding-center orbits in the presence of collisions and other interactions). For these three main parts there exist two independent methods in the code which are benchmarked to each other. In orbit integration, guiding-center equations in straight field line coordinates are used, which leads to complicated but efficient system of equations. These orbits have been benchmarked to the guiding-center orbit solved in Cartesian coordinate system, in which equations are simpler but because of the inaccuracy of the system, a smaller time step is needed and simulations with large ensembles are CPU-expensive. Two different collision models—the binary collision model and collisions with fixed Maxwellian background—exist, and they are benchmarked to each other. Solving the E_r from Eq. (5) has been benchmarked to the method in which E_r is solved by iteration. The latter method is presented in Ref. [24]. Both methods have terminated in same steady-state.

A. Evaluation of the Radial Current $\langle \boldsymbol{j}_{NC} + \boldsymbol{j}_{\mathrm{visc}} \rangle$

In solving Eq. (5), the numerical noise in the resulting E_r arises essentially from the evaluation of the radial current $\langle j_{NC} + j_{\mathrm{visc}} \rangle$ from the particle orbits. Moreover, $\langle j_{NC} + j_{\mathrm{visc}} \rangle$ has a nontrivial dependence on E_r and its time derivative, which makes Eq. (5)

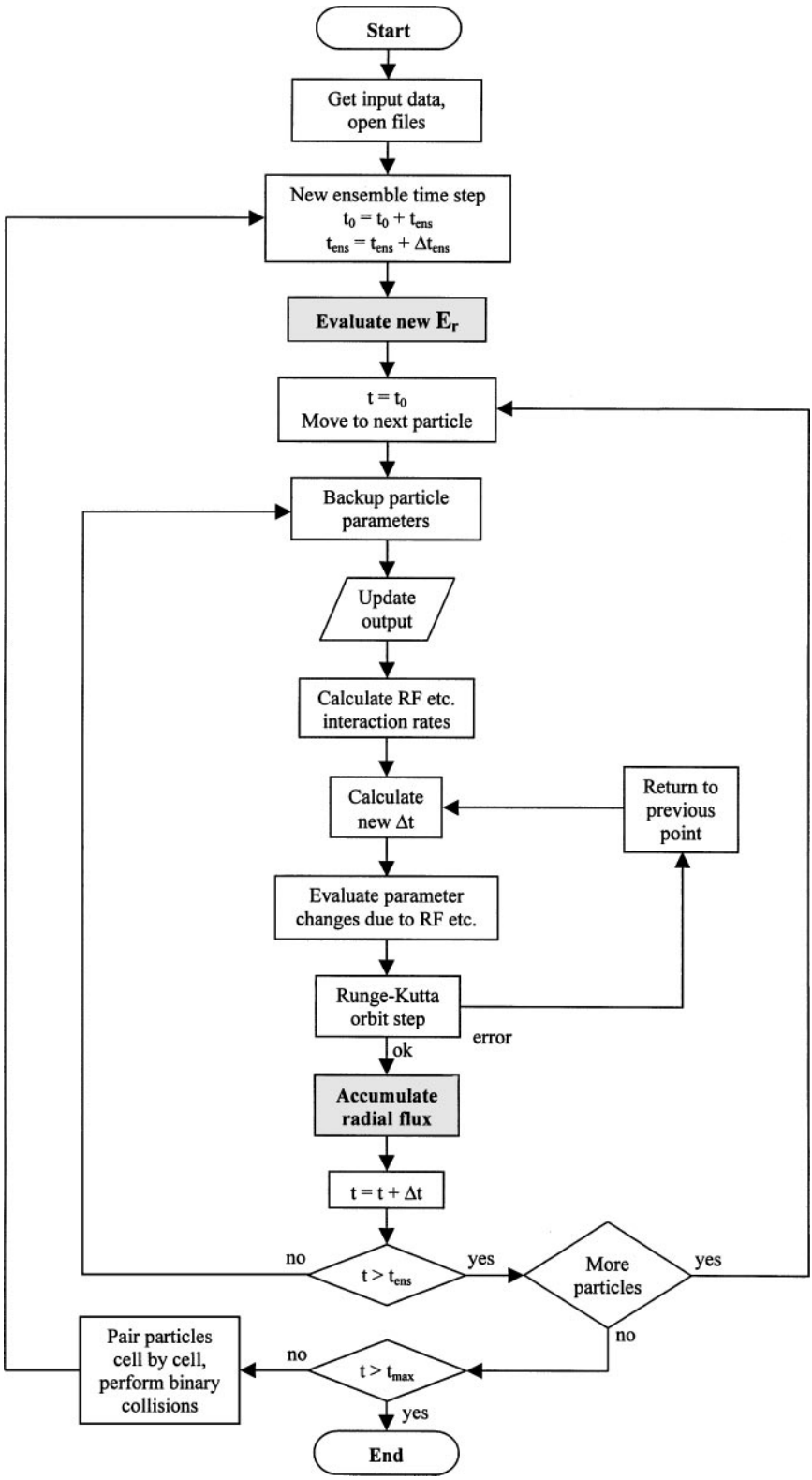

FIG. 2. Flow chart of the ASCOT code.

highly nonlinear, and its numerical solving complicated. The radial net movement of the ensemble by collisions is known to be slow in comparison with the faster collisionless bounce motion of the individual ions in a torus. Locally, this bounce motion provides both inward and outward radial flux which cancel out and thus makes evaluation of the radial current statistically demanding. On the other hand, magnetic ripple, interaction with waves, and orbit losses can provide fast outward motion contained in or added to the bounce motion, and this may significantly exceed the weak collisional flux of the ions.

In the following, $\langle j_{NC} + j_{\rm visc}\rangle$ is calculated on a grid ρ_ℓ, $\ell = 1, ..M$. The grid ρ_ℓ is defined as $\rho_\ell = (\ell - 0.5)ds$ for $\ell = 1, ..M$, where $ds = a/M$. The simulation is split into *global* time steps Δt, during which the ions take numerous *integration steps* along their orbits and suffer collisions, and after which the net radial current is evaluated. Instead of evaluating the current simply as the number of ions crossing the ρ_ℓ-surface per unit time, we obtain the ion flux from the net radial displacement of the ions inside a volume element ΔV_ℓ. This naturally reduces the statistical noise in the ion flux.

The radial current $\langle j_{NC} + j_{\rm visc}\rangle$ is thus obtained as the summation

$$\langle j_{NC}(\rho_\ell, t_i) + j_{\rm visc}(\rho_\ell, t_i)\rangle = \sum_k \frac{e \times d\rho^{*i}_{k,\ell} p_k}{\Delta t A_\ell ds}. \tag{6}$$

Here, index i denotes the ith timeslice, $t_i = i\Delta t$, index ℓ denotes the ℓth radial surface, and index k runs through the test particle ensemble. The radial displacement $d\rho^{*i}_{k,\ell}$ is the fraction of the total radial motion $d\rho^{i}_{k,\ell}$ minus the polarization drift step that the kth particle makes between $\rho_\ell - 0.5$ ds and $\rho_\ell + 0.5$ ds during the ith time step. A_ℓ is the flux surface area at ρ_ℓ. The weight factor p_k is equal to the total number of ions in a real configuration represented by the kth test particle. The radial current is thus the sum of the steps $d\rho^{*i}_{k,\ell}$ of the unpolarized radial motion of the test ion multiplied by its charge e during each passage of the particles in the ensemble through the differential flux surface volume element ΔV_ℓ around the radius ρ_ℓ. The ion density and poloidal and toroidal rotation mass flows can be evaluated accordingly by replacing $ed\rho^{*i}_{k,\ell}/|\nabla\rho|$ by $dt^{i}_{k,\ell}$, $m \times d\theta^{i}_{k,\ell}$, and $m \times d\phi^{i}_{k,\ell}$, respectively, in Eq. (6). Here, $dt^{i}_{k,\ell}$ is the fraction of time the test particle k spent in the volume element ΔV_ℓ during the ith global time step, and $d\theta^{*i}_{k,\ell}$ ($d\phi^{*i}_{k,\ell}$) is the fraction of the total poloidal (toroidal) movement it made within the volume element ΔV_ℓ during the ith global time step.

Figure 3 shows the convergence test for the radial current with the ensemble size in a homogeneous plasma as calculated by this method for a fixed E_r together with fixed plasma background for the collisions. Efficient convergence is demonstrated.

B. Solving the Electric Field

The radial electric field E_r is solved from Eq. (5) using a first-order integration scheme in time on the same grid used for the evaluation of $\langle j_{NC} + j_{\rm visc}\rangle$. The field at t_{i+1} is given by the array $E^{i+1}_{r,\ell}$ obtained from the time integral of Eq. (5),

$$E^{i+1}_{r,\ell} = E^{0}_{r,\ell} - (1/\alpha)\sum_i \sum_k \frac{ed\rho^{*i}_{k,\ell} p_k}{A_\ell ds}. \tag{7}$$

Here, the array $E^{0}_{r,\ell}$ gives E_r at $t = 0$ which is the start of the simulation. The sum over i runs through all global time steps from $t = 0$ up to the $(i + 1)$th time step. The

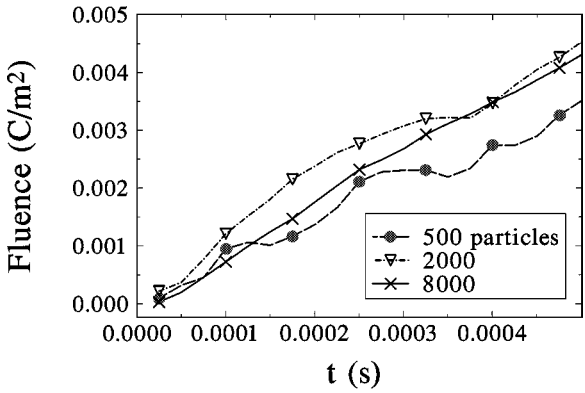

FIG. 3. Convergence test of the fluence calculation using different ensemble sizes. Homogeneous toroidal plasma with $n = 5 \times 10^{19}$ m^{-3}, $T = 200$ eV, $R = 1.65$ m, $B = 2.5$ T, and $B_p = 0.25$ T is assumed. The fluence is measured at the center of a radial annular simulation region from $r = 0.15$ m to $r = 0.35$ m.

method is first order because the orbit tracing; i.e., the evaluation of the radial displacement $d\rho^{*i+1}_{k,\ell}$ is obtained using $E^i_{r,\ell}$ from the previous global time step in calculating the drifts. Comparing the first-order integration scheme with the second-order scheme that involves iterative solution method for $\langle j_{NC} + j_{\text{visc}} \rangle$ and E_r, both calculated consistently up to the $(i + 1)$th time step, did not show any significant difference in accuracy for the applied time steps with simulation periods of a few milliseconds.

Because the viscosity drift v_{visc} is proportional to the second-order radial derivative of E_r, boundary conditions for E_r are required. Because of this same term, the time step dt in the simulations is restricted by the Courant condition $dt < ds^2/(2\eta|\nabla\rho|^2)$, making calculations with very high η impractical. However, using the Braginskii viscosity coefficient defined in Section II, this constraint is not very severe, but the time step is restricted by the more stringent requirements of having sufficiently many integration steps during the bounce period of the orbits and having the time step well shorter than the collision period. The spatial grid size is important because it determines the resolution of E_r obtained and sets a lower limit for the ensemble size. With the chosen method for accumulating particle flux, a coarser grid gives a better statistical accuracy for the current evaluation.

C. Initialization of the Particle Ensemble

In Monte Carlo orbit following codes, it is usually straightforward to initialize the particles in the configuration and velocity space according to requirements of the problem. In practice, an ion ensemble that corresponds to the main plasma is initially distributed according to the assumed background density $n(\rho)$ and temperature $T(\rho)$ profiles. The test particles are distributed uniformly in radius and in poloidal and toroidal angles. The weight factors assigned to test particles are proportional to the real total particle number contained in the corresponding phase space volumes and in an ensemble thus reflect various macroscopic distributions of the particles, e.g., the density profile. In velocity space, the particles are distributed evenly in the particle pitch $v_\parallel/v$, and randomly in speed according to a Maxwellian distribution that corresponds to the local temperature. In the following, we call this kind of simple initialization a macroparticle initialization. When a fixed neutralizing electron background is assumed, the radial ion density profile remains practically unchanged, provided

that the self-consistent radial electric field is evaluated from the quasineutrality condition. Depending on the collision model, the radial temperature profile of the ensemble may nevertheless change (see below Section E) even in the absence of heat sources.

With the basic initialization described above, a problem arises in evaluating $\langle j_{NC} + j_{\mathrm{visc}} \rangle$ for strongly inhomogeneous plasmas. This is a consequence of the finiteness of the particle orbits. Consider an annular volume element ΔV_ℓ. Test ions launched near its inner edge have significantly larger weight (corresponding to higher density) than ions originating from its outer edge. Consequently, in the initial phase of a bounce period, there can transiently exist a finite net current even with closed orbits and no collisions. This transient current decays away with oscillations on a few bounce time scale, but may severely perturb the solution for the E_r dynamics. This can be avoided by initializing the ions in the invariant space that spans the different particle orbits. In the presence of collisions, the particles cannot complete the orbits which makes a proper initialization of the orbits computationally extremely difficult. Because avoiding any unphysical radial current is of primary importance for solving E_r, an initialization on collisionless orbits is adopted here. This guarantees that no current arises at the start from the radial inhomogeneity (and related weight factor variation) even in the presence of collisions. On a bounce time scale, with such an initialization the presence of collisions may, however, lead to some modifications of the originally adopted n and T profiles, which persist for the rest of the simulation.

In a torus, with closed nested magnetic surfaces the collisionless particle orbits are closed trajectories on a poloidal cross section. An example of such a trajectory is sketched in Fig. 4b. In an axisymmetric torus, three orbit invariants are sufficient to specify an orbit. Such invariants can be, for example, particle total energy, magnetic moment, and particle pitch or poloidal angle at a given special point on the orbit [26]. In a collisionless plasma, the

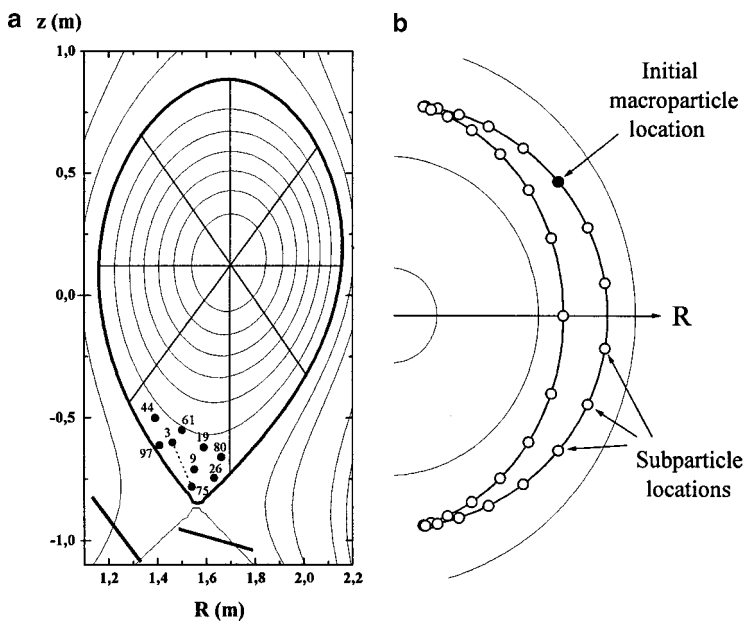

FIG. 4. (a) Poloidal cross sections of the cells used for macroparticle initialization in the plasma region. The scheme of binary collision model is depicted in a cell on the bottom. (b) Subparticle initialization on a collisionless particle orbit.

ensemble initialization can be made in a phase space formed by such invariants. However, in a torus, this has been found to be nontrivial [26].

A convenient way to provide the ion ensemble with a uniform orbit initialization is to introduce *subparticles*. This method also avoids the problems related to mapping of the invariant space. In the subparticle method each original test particle, called a *macroparticle* here, is replaced by N subparticles with a weight equal to $1/N$ times the macroparticle's weight, and the subparticles are distributed on the orbit of the original macroparticle. On the orbit the initial distribution of subparticles is uniform in bounce time; i.e., the time taken by a particle to traverse the orbit segment between two neighboring initial positions of the subparticles is invariant. This is shown schematically in Fig. 4b.

In the code, first the macroparticles are identified and their weight is specified as described in the beginning of this section for macroparticle initialization. Next, the corresponding orbit trajectory of each macroparticle is calculated by solving numerically the equation for the guiding-center motion until the orbit has become fully closed on the poloidal cross section. Thereafter, the subparticle locations and velocities for initialization on this orbit are determined, with the condition that the subparticles follow this orbit during their collisionless guiding-center motion. The actual Monte Carlo calculation is then performed with the ensemble consisting of the created subparticles and their weights. For collisionless calculations, this kind of initialization has been found to reproduce the macroscopic particle distributions obtained by the alternative macroparticle initialization (where no splitting to subparticles is made) at steady state. The required number of subparticles vs. each orbit for good cancellation of the transient radial currents of the particles after intialization has been obtained to be relatively large; $N = 50$–100. However, at the same time the number of orbits (i.e., of the original macroparticles) for subparticle initialization can be reduced so that the total size of the ensemble can be kept comparable in both macroparticle and subparticle initializations.

Figure 5 shows the time evolution of the radial E_r-profile for the subparticle initialization together with a result where no particle splitting was applied. The field was calculated for an FT-2 [14] tokamak plasma under H-mode conditions, where a strong density gradient exists. With the subparticle method, 50 subparticles per orbit were applied and $E_r = 0$ at $t = 0$ was assumed. With subparticles, the field develops much more smoothly than with the conventional initialization and without oscillations to an equilibrium, where strong oscillations and a rapid drop down to large negative E_r-values at the very start are observed. This is because in FT-2, because of its high poloidal Mach number $|E_r/B_p v_T|$, even at modest values of E_r, the system evolution is sensitive to both the initial value $E_r(0)$ and the start-up phase of the solution (see Section IV). In the subparticle method, the initial radial current stays negligible ensuring a slow variation of E_r from its initial value. The subparticle method thus provides a *quiescent start* for the simulations and avoids the unphysical variation of E_r by the numerical radial currents imposed by the weight-factor inhomogeneity. With splitting, the orbit loss brings E_r down to large negative values at a later stage. This can be seen in Fig. 5a, where the field evolution, in agreement with the orbit loss mechanism, starts near the separatrix and subsequently moves further inside. The state (still evolving in Fig. 5a) at $t = 200$–300 μs is almost double in $|E_r|$-value compared to the case with conventional initialization. Thus, the initialization method adopted is important for the system evolution to steady-state. It should, however, be emphasized that the sensitivity to the initialization is peculiar to configurations where the poloidal Mach number becomes large (≥ 1) during the field evolution and/or gradient of the background pressure is strong. For ASDEX Upgrade

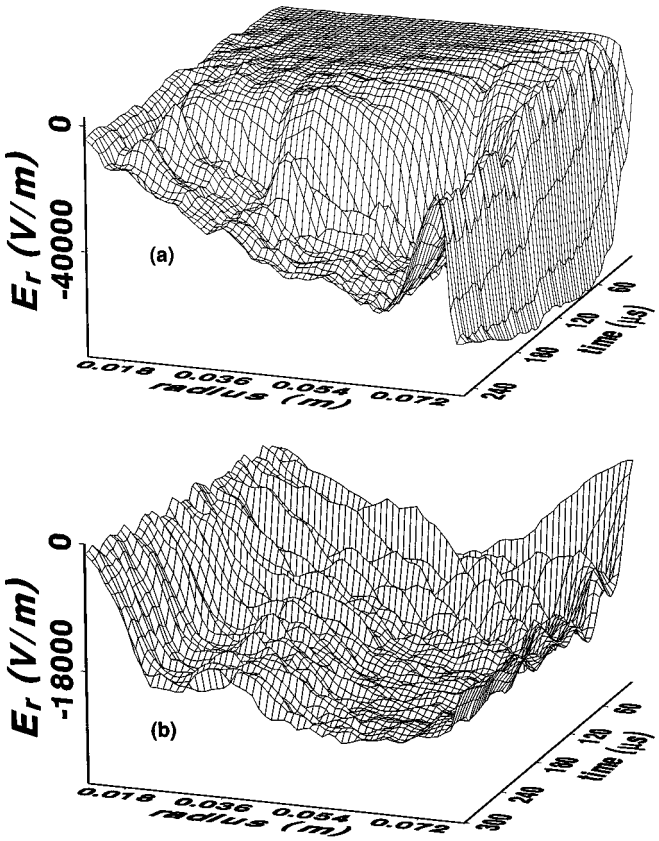

FIG. 5. The evolution of the radial electric field (a) with subparticle initialization and (b) without subparticle initialization in FT-2 tokamak. $R = 0.55$ m, $a = 0.08$ m, $I = 22$ kA, $B_t = 2.2$ T with parabolic current profile and profiles $n(r) = 5 \times 10^{19}[1 - (r/a)^2]^{2.5}$ m^{-3} and $T(r) = 290 \times [1 - (r/a)^2]^{1.3}$ eV. Four million particles are used in both simulations with a time step of 1.5 μs for updating E_r.

configurations with standard discharge parameters, for instance, $|E_r/B_p v_T|$ is almost 10 times smaller than in FT-2, and no such sensitivity was observed when the ambipolar neoclassical E_r [4] was used as an initial condition. These results will be further discussed in Section IV.

It is worth noting that for orbits intersecting the vessel wall or divertor plates/limiter, the distribution of subparticles is nontrivial. In principle the particles with orbits intersecting the plasma facing components should not reenter the plasma and, therefore, the subparticles should not be initially distributed on the section of these orbit on which the particles are moving inward from the separatrix. However, for collisional plasmas such an initialization may overestimate the initial orbit loss current since the particles cannot complete the trajectories. Therefore, to ensure a smooth initialization, a full distribution of subparticles on the orbits inside the plasma is applied even on the orbits intersecting the plasma facing components.

D. Boundary Conditions

As already implied by Fig. 5, the entire plasma cross section is not necessarily needed to investigate the relevant physics. The radial electric fields related to L-H transition and

formation of ITBs, in particular, have radial extent of only a few centimeters even in large machines like JET and ASDEX Upgrade. Therefore, the computational effort is reduced enormously by restricting the simulation to a relevant region $\rho_L < \rho < \rho_R$ in minor radius. Whenever there are no special constraints at the boundaries ρ_L and ρ_R posed by the problem, and when the mass flow parallel to the magnetic field is given at the boundaries, E_r can be evaluated in the region $\rho_L < \rho < \rho_R$ by using the well-known neoclassical analytical ambipolar value $E_a(\rho)$ [4] as the boundary condition at $\rho = \rho_L$ and $\rho = \rho_R$. If the outer boundary lies outside the separatrix, $\rho_R > \rho_s$, $E_r(\rho_R) = 0$ is used.

The boundary conditions at ρ_L and ρ_R may affect the E_r profile inside the simulation region through the gyroviscosity. In order to test this effect, the value of E_r at the outer boundary was varied in a large range to show that the chosen value does not have significant effect on the results. Simulations were done with boundary conditions $E_r(\rho \geq \rho_s) = +20,\ 0$, and -40 kV/m for the ASDEX Upgrade edge parameters in the case which will be described in Section IV.A. Since the viscosity depends on the second derivative of E_r its effect is to bend the profile to the boundary value. As the neoclassical gyroviscosity is very weak, the E_r profile is affected only within $\Delta\rho \approx 0.003$, which is less than 2 mm inside the separatrix. However, if the viscosity is anomalous, the effect of the boundary condition extends further inside, making the profile smoother.

As for the particles at the boundaries, whenever ρ_L and ρ_R lie inside the the plasma, the outflowing particles are reflected at these boundaries. This is accomplished by following the orbits for $\rho < \rho_L$ and $\rho > \rho_R$ in the absence of collisions, gyroviscosity drift, and polarization drift and by stopping the clock during the time the particles spend in these regions. This is consistent with the assumption of no source of toroidal momentum and zero radial current for $\rho < \rho_L$ and $\rho > \rho_R$.

The ions are initialized within $\rho_L < \rho < \rho_R$, and those hitting the divertor or wall outside $\rho > \rho_R$ are promptly reinitialized at $\rho = \rho_R$. The reinitialization is uniform in pitch and poloidal angle, with the local Maxwellian velocity distribution. This reinitialization does not create any physical current in the simulation domain and, being more uniform (in phase space) than the loss process, it simulates well the replacement of charge lost through the separatrix. This method has been successfully applied recently, with the outer boundary at the separatrix, $\rho_R = \rho_s$, to calculate [12] the orbit loss, as well as the related source of poloidal rotation and its dynamics for L-H transition conditions in ASDEX Upgrade [15].

Whenever the scrape-off-layer plasma outside the separatrix ρ_s is simulated, i.e., $\rho_R > \rho_s$, and there are plasma facing components between ρ_s and ρ_R, particles hitting these components are reinitialized still uniformly in pitch and poloidal (and toroidal) angle, but now the magnetic surface of the reinitialization is the same where the particle hits the component. This ensures that no radial current is generated by the reinitialization, and quasineutrality holds everywhere.

E. The Collision Operator

In the past, most particle simulations using Monte Carlo collision operators have assumed a fixed plasma background for the test particles to collide off. Although such operators do not conserve momentum nor energy, it has been possible to calculate, for example, diffusion coefficients for collisions between unlike particles (or between minority and majority species). To study the relaxation of plasma rotation in tori, however, the momentum conservation in collisions is expected to be important.

In order to properly treat the momentum equation and momentum generation, a binary collision model [13] that conserves momentum and energy in pairwise collisions between the ions has been implemented in the ASCOT code. In the poloidal plane the simulation region is divided into small cells so that the plasma parameters do not vary significantly inside the cells. Particles in each cell are randomly paired, and small angle collisions are performed pairwise. The adopted collision operator conserves the number of particles, the total momentum, and the total energy quasi-locally. This model was recently tested [21] by calculating poloidal rotation relaxation rates for a homogeneous plasma and by comparing the perpendicular conductivity and parallel viscosity evaluated by ASCOT with the analytical expressions [27, 28]. The simulations were carried out for a wide range of collisionalities and rotation velocities.

The problem with an energy-conserving collision model for total f-schemes is that the temperature profile is not sustained by the ensemble without introduction of a proper energy source/loss for the simulation particles. Therefore, in some cases it is useful to let the particles collide with a fixed background without conserving energy or momentum. Under such conditions, the collisions themselves automatically provide the source and sink of heat and sustain the given temperature profile of the ensemble. Figure 6 shows a comparison of steady-state radial E_r profiles obtained for the plasma periphery in ASDEX Upgrade using the binary collision model and the collision operator that assumes a fixed plasma background. The steady-state solutions obtained are very similar, indicating that momentum conservation does not play an important role in problems where the poloidal rotation is supported by the orbit loss current. This is because, as a result of the orbit loss, the poloidal rotation cannot relax by generating parallel flow intermediated by momentum conservation in collisions [21].

The binary collision model is used as a default in ASCOT, but also an option for collisions with fixed background is included for benchmarking and some special purposes. There is no significant difference in computation speed between the collision models. In the problems in which the E_r profile is solved at the plasma edge in the presence of ion orbit loss mechanism, however, the collisions with fixed background are more suitable than the binary collision model in longer runs if the aim is to obtain the result for a given temperature profile. When the energy-conserving collision operator is used, the plasma would indeed cool all the

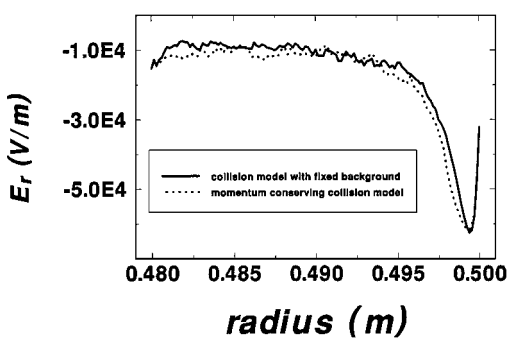

FIG. 6. Comparison of the steady-state E_r-profiles between the simulations run with the momentum (and energy) conserving binary collision operator and with an operator making collisions with a fixed background. ASDEX Upgrade parameters $R = 1.65$ m, $a = 0.5$ m, $B_t = 2.5$ T, $I = 1$ MA with a parabolic current density profile and linear ramps from $n = 4 \times 10^{19}$ m^{-3}, $T = 200$ eV at the separatrix to 1.9 times larger values at 2 cm (on the equator) inside from the separatrix.

time since the lost particles, which are mainly energetic, are replaced by thermal particles reinitialized at $\rho = \rho_R$. Thus, to maintain the experimental radial temperature, we rather heat the plasma with the test particle collision operator, which assumes fixed Maxwellian background. Both methods give the same quasi steady-state E_r profile if the simulation time is short compared to the time in which the temperature profile changes significantly.

The binary collision operation is performed at specific time instants for the whole particle ensemble together with evaluation of macroscopic particle distributions and updating of the radial electric field from Eq. (5). The interval (global time step) between these instants is taken a small fraction of the minimum of collision and bounce times of particles in the ensemble, and is typically in the range of 0.1–10 μs. With fixed background collision operation, each particle can be operated separately at specific time instants during their guiding-center motion. Again, the interval between these instants is taken a small fraction of the minimum of collision and bounce times of this particle at that time. Typically, 25–100 collision operations are performed during each bounce of the particle.

IV. SIMULATION OF NEOCLASSICAL PLASMAS FOR CONDITIONS WITH TRANSPORT BARRIER

In the following, the present simulation method is applied both to simulate globally the radial electric field in the FT-2 tokamak for L-mode and H-mode conditions and to evaluate locally the sheared neoclassical $\mathbf{E} \times \mathbf{B}$ flow at the edge region of ASDEX Upgrade for L-H transition conditions. As the outer boundary, both simulations use the separatrix or the radius at the limiter. In the SOL region, the ions are followed until they hit the plasma-facing components (limiter, divertor plate, or wall), and after that they are regenerated at the outer boundary as explained in the previous section. Because the radial current is taken zero, no large rotation is assumed as an initial condition, and no toroidal momentum source is adopted in the present scheme, no significant parallel flow generation takes place and, consequently, momentum conservation will not be an issue, and collision operators with fixed plasma background will be used in the following examples.

A. Edge Plasma Simulation for the L–H Transition in ASDEX Upgrade

The ASDEX Upgrade [15] tokamak has the minor radius $a = 0.5$ m, major radius $R = 1.65$ m, elongation 1.6, plasma current $I = 1$ MA, and the toroidal magnetic field $B_t = -2.5$ T. Corresponding to the discharge 8044 (a deuterium plasma), a separatrix density 1.2×10^{19} m^{-3} and temperature 140 eV with about 1.9 times larger values at 2 cm inside the separatrix are adopted for reference. The radial electric field is initialized to its neoclassical ambipolar field (assuming zero parallel average mass flow)

$$E_{NC} = (k_B T/e)(n'/n + \gamma T'/T), \tag{8}$$

where the primes denote radial derivative, and γ, given in Ref. [4], depends on the collisionality. In minimum 200,000 simulation (sub-)particles are distributed along the sections of the ion orbits that lie within the 2-cm wide simulation region. The global time step used

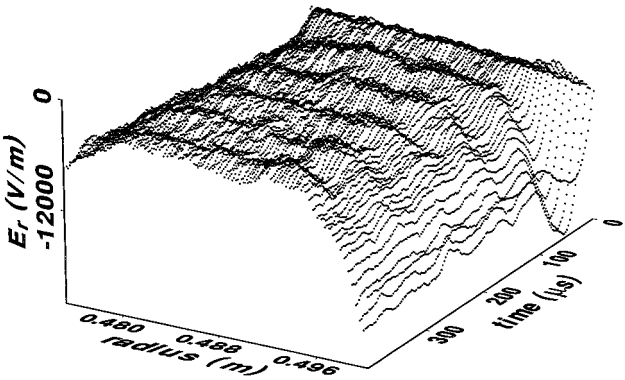

FIG. 7. The evolution of the radial electric field without subparticle initialization for the ASDEX Upgrade with parameters $R = 1.65$ m, $a = 0.5$ m, $B_t = 2.1$ T, $I = 1$ MA with a parabolic current density profile and linear ramps from $n = 1.2 \times 10^{19}$ m^{-3}, $T = 120$ eV at the separatrix to 1.9 times larger values at 2 cm (on the equator) inside from the separatrix. 3.2 million simulation particles using a time step of 2.5 μs and the radial grid size 0.3125 mm (on the equator) for updating E_r. Neoclassical ambipolar E_r value with $\gamma = 1.5$ is used at the left boundary and at the initialization of E_r.

for advancing the electric field is 1.25 μs. For most of the orbits, more than four integration steps are used to advance the particle orbits within each step. Figure 7 shows the evolution of the E_r profile in the region $0.96 < \rho < 1$ ($\rho_R = 1$) and indicates, in a millisecond time scale (i.e., within a few collisional times and a few bounce times), the formation of a strong, sheared inward field near the separatrix. The numerical value for E_r on the outboard equator can be obtained using $d\rho/dr = 2$ m^{-1}. Deeper inside the plasma, the field remains close to its initial, analytical ambipolar value. The inaccuracy in determining γ for given n and T profiles from the expressions in Ref. [4] explains the overshoot of E_r at the beginning of the simulation and the related temporal oscillation of the E_r profile that is damped during the simulation. The field enhancement near the separatrix has recently been interpreted [12, 29] to arise from the ion orbit loss and the radial current related to it: a larger inward E_r (in comparison to the neoclassical ambipolar value) is required to drive diffusive current inward to balance the orbit loss current as sketched in Fig. 1. It is of interest to note that the calculation remains stable and a steady-state is achieved at an instantaneous noise level of 5–10 % for the present simulation with 3.2×10^6 simulation particles. For steady-state conditions, it has been possible to further reduce this noise by simple time-averaging of the resulting E_r profiles from sufficiently long runs.

Figure 8 shows steady-state E_r profiles for various separatrix T-values obtained by a scalar multiplication from the reference profile. The analytical ambipolar profiles $E_a(\rho)$ are shown for comparison. The analytical values are based on a number of assumptions made in deriving the expression from the drift-kinetic equation [4]. The present simulation is carried out for fairly steep plasma gradients, with particle orbit widths w comparable to the gradient scale length L_g, while the theory in Ref. [4] is based on the assumption $w \ll L_g$. At the lowest temperature, the enhancement of E_r is weak, as expected from the orbit loss model, and the field remains close to the analytical value. For increasing edge temperature and edge temperature gradient, the simulated field becomes strongly sheared and, indeed, the $\mathbf{E} \times \mathbf{B}$ shear becomes sufficient for turbulence suppression [12] at L–H transition conditions ($T(\rho_R) = 120$ eV) of ASDEX Upgrade.

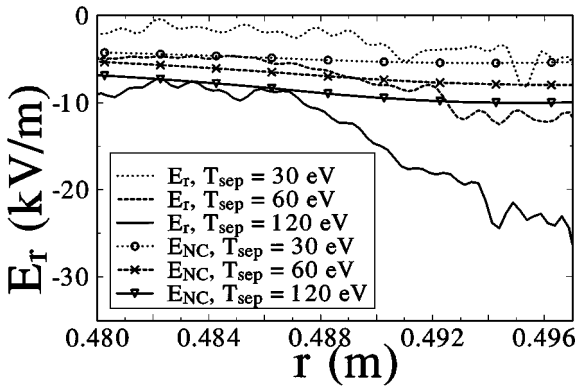

FIG. 8. Steady-state radial electric field profiles at various separatrix temperatures for the ASDEX Upgrade with the separatrix density 1.2×10^{19} m^{-3} and 1.9 times larger temperature and density values at 2 cm (on the equator) inside from the separatrix. The neoclassical ambipolar values from Eq. (8) are shown for comparison. 200,000 simulation particles were used.

B. Neoclassical Electric Field in FT-2 Tokamak

On FT-2 tokamak ($R = 0.55$ m, $a = 0.08$ m, $I = 22$ kA, $B_t = 2.2$ T), a spontaneous transition to improved confinement mode has been observed in the presence of lower hybrid heating [14]. The barrier is believed to form as a result of a strongly sheared electric field E_r. The small plasma current leads to trapped orbits with very large banana widths, on the order of the minor radius. Also, the toroidal ripple is large, and the ripple-loss region extends deep into the bulk plasma. Both of these features can lead to significant direct orbit losses, and therefore it is suggested that purely neoclassical effects might explain the formation of a radial electric field with significant enough shear to suppress turbulence.

We have simulated the generation of the radial electric field in FT-2 geometry. The simulations cover the entire plasma up to the limiter radius at ρ_R, and they are carried out for two different plasma conditions: for poor confinement characteristics (dubbed *L-mode*) and for improved confinement characteristics (dubbed *H-mode*). The corresponding plasma profiles are shown in Fig. 9. As in the ASDEX Upgrade study, the collision model with fixed electron and ion backgrounds is used. The ions are followed in the scrape-off-layer (SOL) until they either intersect the wall or the limiter or return to the main plasma. The limiter is simply defined as a region in the SOL limited by two poloidal angles: $\theta_{L,low} < \theta < \theta_{L,high}$ with $\theta_{L,low} = -68^\circ$ and $\theta_{L,high} = -22^\circ$.

Figure 10 gives the smoothed-out E_r profiles from a 0.5-ms-long simulation (with a 0.75-μs global time step) that used 800,000 test particles (hydrogen) for both L- and H-mode cases. The simulation time was sufficient for obtaining a steady state (compare Fig. 5). The noise in these simulations was somewhat larger than in the ASDEX Upgrade edge plasma simulation for reasons discussed below. The neoclassical ambipolar E_r profiles from Eq. (8) are shown for comparison. For the L-mode, the field remains close to the predicted ambipolar value in most of the simulation region. At outer regions, close to the limiter radius, a modest enhancement in the field is observed. On the other hand, for the H-mode case a strongly sheared field structure with a significant deviation from the ambipolar values is obtained.

It is important to note that for the L-mode, the Mach number of the poloidal rotation $|E_r/B_p v_{ti}|$ is close to one, and for the H-mode case it is well in the supersonic region.

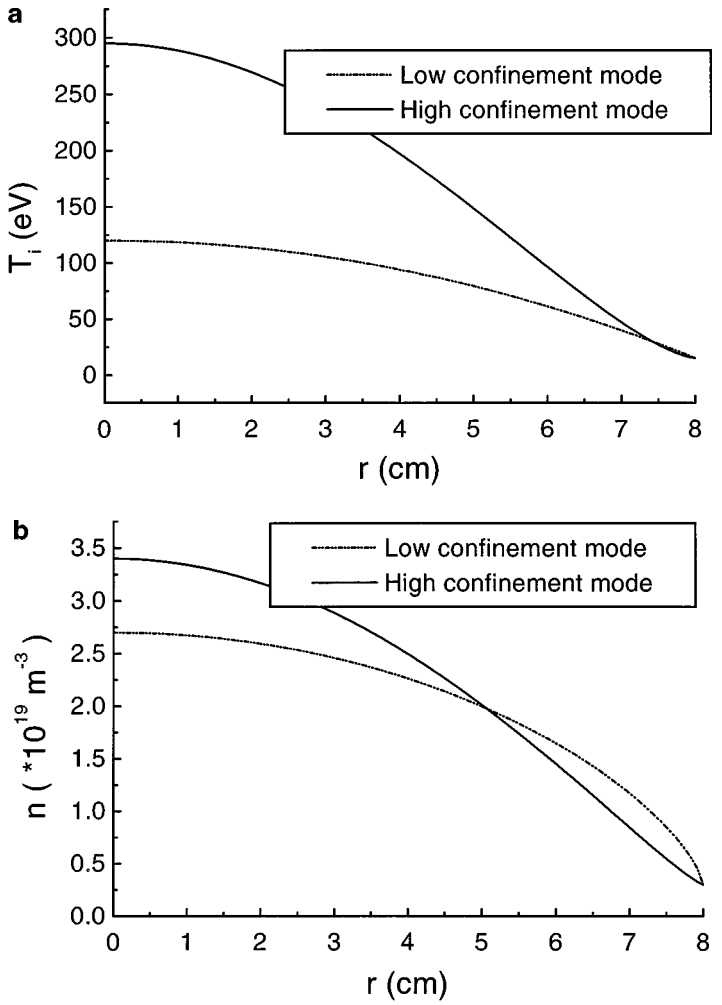

FIG. 9. (a) Temperature and (b) density profiles used for the FT-2 simulations in L-mode and H-mode conditions of the experiments.

Consequently, in the H-mode, the $\mathbf{E} \times \mathbf{B}$ rotation in the poloidal direction is so strong that it completely dominates the poloidal motion arising from the thermal parallel motion. Thus, the orbit widths become strongly squeezed. This, together with the steep gradients (in comparison to the orbit widths in the absence of E_r), indicates that the standard neoclassical theory is not valid. Because the orbit widths are strongly squeezed, the enhancement in E_r for the H-mode case here does *not* have its origin in the orbit loss (although the effect of orbit losses can be seen near the limiter), but is a direct consequence of the neoclassical ambipolar balance, the description of which requires a much more complete analytical treatment than hitherto presented in the literature. It should be mentioned that the order of magnitude of E_r and its gradient were obtained independent both of the initial conditions ($E_r = 0$ or $E_r = E_a$) on a bounce time scale and of the initialization scheme.

The E_r structures obtained for FT-2 were found to be prone to a slow numerical instability which was indicated by a steady growth of the field values in opposite directions,

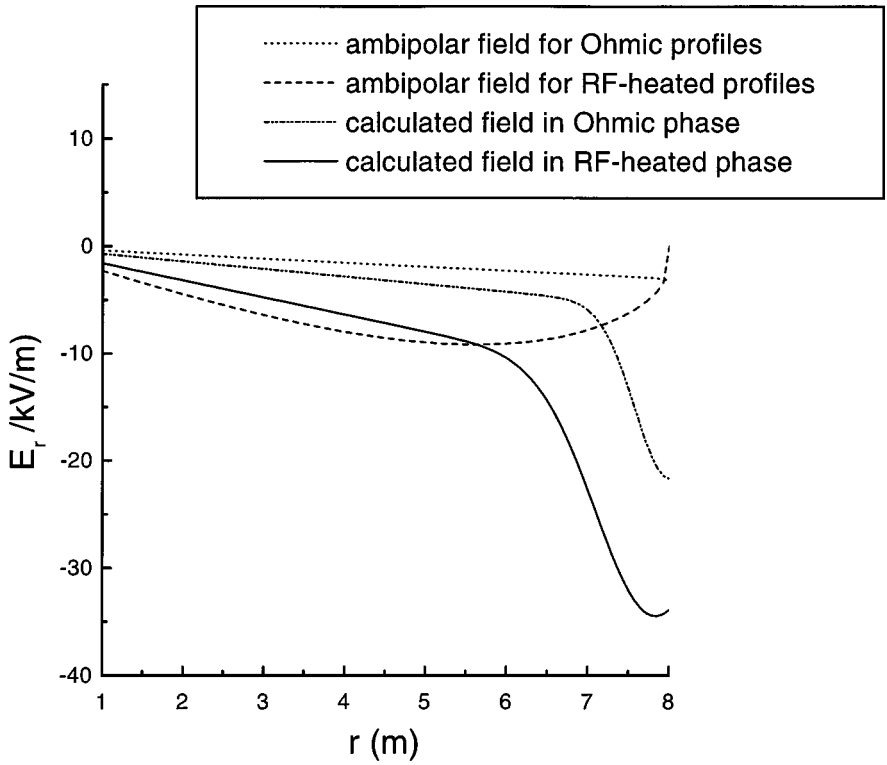

FIG. 10. Smoothed time-averaged profiles of the steady-state radial electric field for the FT-2 L- and H-mode profiles.

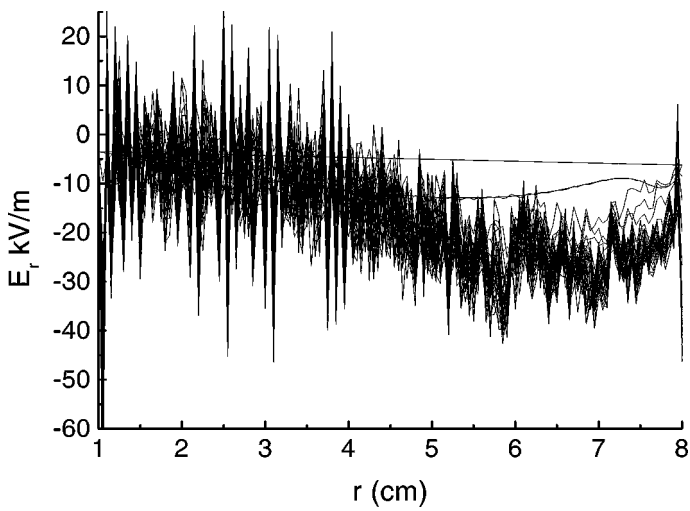

FIG. 11. The snapshot of the radial electric field profile at $t = 500\ \mu$s for an FT-2 simulation for the H-mode profiles using no gyroviscosity enhancement. The unstable spikes appear roughly with a period of the spatial grid size used for evaluation of E_r.

positive and negative, on the consequtive grid points ρ_m and ρ_{m+1}, respectively. This is demonstrated in Fig. 11, which shows the E_r structure for the H-mode case after a 0.5-ms simulation. This uncontrolled (but at later times saturating) grid instability was not found to be suppressed by a diminishing time step dt nor by the increase of ensemble size. An iterative second-order time integration of Eq. (5) was not helpful either. It was observed that increasing the perpendicular viscosity coefficient η significantly weakens the growth of this instability. The results in Fig. 10 were obtained with a viscosity 50 times the Braginskii viscosity. The appearance of the grid instability in the present FT-2 case is probably connected to the high poloidal Mach number of the rotation at modest E_r amplitude (in contrast to ASDEX Upgrade where no instability was observed and where the Mach number stays below unity), but its mechanism has not been thoroughly explained. The most efficient way to avoid this instability was to evaluate the fluence in Eq. (7) by averaging its value over the three neighboring grid cells $\ell - 1$, ℓ, and $\ell + 1$ around ℓ in advancing to $E_{r,\ell,i+1}$. This prevents the positive feedback between the electric field energy and the observed unstable collective motion of the ions toward the grid knot points: at such a grid point, in the absence of the averaging, the electric potential grows, the kinetic energy of these ions decreases and, because of the high poloidal Mach number, the ions become highly localized and attached to that radius.

V. CONCLUSIONS

Using the neoclassical radial current balance (quasineutrality condition) with the polarization current in a Monte Carlo particle following code, it is demonstrated that neoclassical rotation dynamics and the radial electric field can be resolved in a torus without resorting to a full solution of the Poisson or Maxwell equations. Filtering the turbulent fields in this way out reduces the computational effort significantly and makes the neoclassical phenomena more transparent. However, the present reduced model has indicated a number of important elements which must be shared also by the full model, for example, the gyrokinetic simulation, if one wishes the proper neoclassical behavior to be simulated. There are specific requirements for the time step, grid size, ensemble size, particle initialization, and reinitialization, as well as for boundary conditions, which must be satisfied for proper description of particle and heat flux in the presence of steep gradients, finite orbit widths, and orbit losses.

It was shown that the solving of the polarization equation (5) for E_r can be kept stable, even with the first-order explicit integration scheme, provided the poloidal Mach number $|E_r/B_p v_T|$ remains well below unity. With typical tokamak parameters relevant for fusion studies, the integration accuracy is acceptable for several millisecond integration runs using some tens of time steps per orbit bounce and collision time and ensembles containing about thousand particles per radial grid cell applied for resolving E_r profile. The method remained stable and accurate with the presence of orbit losses, and the first self-consistent neoclassical radial electric field profiles were produced for conditions relevant for transport barrier formation with large E_r shears. However, the polarization equation becomes numerically unstable if the Mach number becomes of the order of unity or larger. This instability has been found to arise from the ion collective attraction to grid points where the electric potential grows, and where the ions lose their kinetic energy, the latter being transformed to the electric potential energy thus reinforcing the potential growth, and become

frozen at this radial location by increased orbit squeezing as a result of the increased $|E_r|$. It was not possible to stabilize this instability by decreasing time step, increasing ensemble, by changing the grid size, or by using implicite integration schemes. The increase of gyroviscosity restrains the instability, but the most efficient way to suppress it has been by averaging the flux in Eq. (5) over the three neighboring radial grid cells in advancing E_r in Eq. (5).

With large orbit widths, steep gradients, and a large poloidal Mach number, the solutions have been found to become sensitive to the initialization. Although the proper initialization is not possible without knowing the very solution, orbit initialization, i.e., distributing the ensemble particles uniformly on the particle collisionless orbits, has been found useful for the solving of the polarization equation. It is important to note that this problem is an issue for any solving method of the particle distribution function, and should be taken into account in toroidal plasma simulations, whether containing turbulence physics or not. With the orbit initialization, one can avoid the unphysical radial flux arising in the starting phase of the particle bounce motion in an inhomogeneous plasma. This then prevents any uncontrolled change of E_r at this stage.

It should be noted that in the radial current balance, one can also include external current, e.g., currents running in a probe shaft extending into the plasma region. In such a case, the current running in the plasma compensates the current in the shaft. The nonzero current in the plasma creates a toroidal $\vec{j} \times \vec{B}$ force which drives momentum and rotation in that direction. Here, the momentum conservation in collisions is important. The latter can be taken into account in the present method with a binary collision technique, as was described in the text. Using the present code, the biased probe excitation of the L–H transition in the TEXTOR tokamak was successfully modeled [12]. Here, in good agreement with the theory, production of propagating soliton-like E_r structures was observed for the first time in simulations.

Examples shown in Section IV demonstrate the power of the present simulation method. Both in small- and medium-sized tokamaks, the neoclassical radial electric field has been solved under conditions close to the transport barrier formation. The observation of large shears in E_r even without bifurcative transition indicates that the neoclassical mechanisms can play an important role in the creation of transport barriers. Various nonambipolar fluxes such as ripple loss, orbit loss, rf-induced fast ion flux, MHD mode generated flux, flux resulting from stochastic magnetic field lines, flux arising from charge exchange collisions, and probe excited flux can be included straightforwardly and investigated. Moreover, the neoclassical equilibria can be obtained with arbitrary initial conditions. It is not difficult to extend the present method to include the electron dynamics by solving the electron and ion orbits together and evaluating their total current for Eq. (5). However, as here the particle radial distribution evolves, special care must be exercised in reinitialization of the particles and in providing a heat source. Such a problem was already considered in the context of biased probe excitation of E_r [12], where reinitialization at both boundaries of the simulation region was mandatory.

ACKNOWLEDGMENTS

This work benefitted from the computing resources of the Centre of Scientific Computing in Espoo, Finland. The authors thank S. Lashkul, K. C. Shaing, and R. Sydora for their valuable comments and discussions in the course of this work.

REFERENCES

1. K. T. Tsang, Y. Matsuda, and H. Okuda, *Phys. Fluids* **18**, 1282 (1975); A. H. Boozer and G. Kuo-Petravic, *Phys. Fluids* **24**, 851 (1981); H.-B. Park, E.-G. Heo, W. Horton, and D.-I. Choi, *Phys. Plasmas* **4**, 3273 (1997); R. E. Potok, P. A. Politzer, and L. M. Lidsky, *Phys. Rev. Lett*. **45**, 1328 (1980); H. E. Mynick, *Phys. Fluids* **25**, 325 (1982); M. Wakatani, *Nucl. Fusion* **23**, 817 (1983); W. Dommaschk, W. Lotz, and J. Nührenberg, *Nucl. Fusion* **24**, 794 (1984); R. H. Fowler, J. A. Rome, and J. F. Lyon, *Phys. Fluids* **28**, 338 (1985); C. D. Beidler, W. N. G. Hitchon, D. L. Grekov, and A. A. Sishkin, *Nucl. Fusion* **30**, 405 (1990), K. Tani, M. Azumi, H. Kishimoto, and S. Tamura, *J. Phys. Soc. Japan* **50**, 1726 (1981).
2. J. M. Dawson, *Phys. Plasmas* **2**, 2189 (1995).
3. W. W. Lee, *J. Comput. Phys*. **72**, 243 (1987).
4. F. L. Hinton and R. D. Hazeltine, *Rev. Mod. Phys*. **48**, 239 (1976).
5. A. M. Dimits and W. W. Lee, *J. Comput. Phys*. **107**, 309 (1993).
6. S. E. Parker and W. W. Lee, *Phys. Fluids* **B5**, 77 (1993).
7. R. D. Sydora, V. K. Decyk, and J. M. Dawson, *Plasma Phys. Contr. Fusion* **38**, A281 (1996).
8. Z. Lin, W. M. Tang, and W. W. Lee, *Phys. Plasmas* **2**, 2975 (1995).
9. R. D. Sydora, *Physica Scripta* **52**, 474 (1995).
10. R. D. Sydora, private communication (2000).
11. S. V. Novakovskii, C. S. Liu, R. Sagdeev, and M. N. Rosenbluth, *Phys. Plasmas* **4**, 4272 (1997).
12. J. A. Heikkinen, T. P. Kiviniemi, and A. G. Peeters, *Phys. Rev. Lett*. **84**, 487 (2000).
13. S. Ma, R. D. Sydora, and J. M. Dawson, *Comput. Phys. Commun*. **77**, 190 (1993).
14. S. I. Lashkul *et al.*, *Proceedings of the 26th EPS Conference on Controlled Fusion and Plasma Physics, Maastricht, 1999, ECA* (European Physical Society, 1999), Vol. 23J, p. 1729.
15. V. Mertens, K. Buchl, W. Junker, F. Mast, M. Schittenhelm, M. Bessenrodt-Weberpals, A. Field, Ch. Fuchs, O. Gehre, O. Gruber, A. Herrmann, G. Haas, A. Kallenbach, H. Kastelewicz, M. Kaufmann, W. Koppendorfer, M. Laux, G. Lieder, J. Neuhauser, F. Ryter, H. Salzmann, W. Sandmann, K.-H. Steurer, A. Stabler, H. Zohm, and the Asdex Upgrade Team, *Proceedings of 20th European Conference on Controlled Fusion and Plasma Physics*, Lisbon (European Physical Society, Petit-Lancy, Switzerland, 1993), Vol. 17C, Part I, p. 267.
16. T. E. Stringer, *Nuclear Fusion* **35**, 1008 (1995).
17. L. Spitzer, *Physics of Fully Ionized Gases*, 2nd ed. (Interscience, New York, 1962).
18. S. I. Braginskii, *Reviews of Plasma Physics* (Consultants Bureau, New York, 1965), Vol. 1.
19. S. V. Novakovskii, A. A. Galeev, C. S. Liu, R. Z. Sagdeev, and A. B. Hassam, *Phys. Plasmas* **2**, 3566 (1995).
20. J. A. Heikkinen and S. K. Sipilä, *Phys. Plasmas* **2**, 3724 (1995).
21. T. P. Kiviniemi, J. A. Heikkinen, and A. G. Peeters, *Nuclear Fusion* **40**, 1587 (2000).
22. T. P. Kiviniemi, J. A. Heikkinen, and A. G. Peeters, *Phys. Plasmas* **7**, 5255 (2000).
23. R. B. White and A. H. Boozer, *Phys. Plasmas* **2**, 2915 (1995).
24. T. P. Kiviniemi, J. A. Heikkinen, T. Kurki-Suonio, A. Peeters, and S. K. Sipilä, *Czechoslovak J. Phys.* **49**, 81 (1999).
25. T. E. Stringer and J. W. Connor, *Phys. Fluids* **14**, 2177 (1971).
26. T. P. Kiviniemi and J. A. Heikkinen, *Comp. Phys. Commun*. **107**, 149 (1997).
27. T. Stringer, *Nucl. Fusion* **33**, 1249 (1993).
28. K. C. Shaing and E. C. Crume, Jr., *Phys. Rev. Lett*. **63**, 2369 (1989).
29. J. A. Heikkinen, T. P. Kiviniemi, and A. Peeters, *Contrib. Plasma Phys*. **40**, 431 (2000).